

Astronomical Notes

Astronomische Nachrichten

Founded by H. C. Schumacher in 1821

Editors

K. G. Strassmeier (Potsdam/Editor-in-Chief),
A. Brandenburg (Stockholm), G. Hasinger (Garching),
R.-P. Kudritzki (Honolulu), T. Montmerle (Grenoble),
R. Neuhäuser (Jena)

WILEY-VCH

REPRINT

Star formation rates and the kinematics of gas in the spiral arms of NGC 628

A. S. Gusev^{1,*}, F. Sakhibov², and Yu. N. Efremov¹

¹ Sternberg Astronomical Institute, Lomonosov Moscow State University, Universitetsky pr. 13, 119992 Moscow, Russia

² University of Applied Sciences of Mittelhessen, Campus Friedberg, Department of Mathematics, Natural Sciences and Data Processing, Wilhelm-Leuschner-Strasse 13, 61169 Friedberg, Germany

Received 2015 Jan 20, accepted 2015 Apr 12

Published online 2015 Jun 10

Key words galaxies: individual (NGC 628) – galaxies: kinematics and dynamics – HII regions – ISM: kinematics and dynamics

The relations between star formation rates along the spiral arms and the velocities of gas inflow into the arms in the grand-design galaxy NGC 628 were studied. We found that the radial distribution of the average star formation rate in individual star formation regions in regular spiral arms correlates with the velocity of gas inflow into the spiral arms. Both distributions have maxima at a galactocentric distance of 4.5–5 kpc. There are no correlations between the radial distributions of the average star formation rate in star formation regions in spiral arms and outside spiral arms in the main disc. We also did not find a correlation between the radial distribution of the average star formation rate in star formation regions in spiral arms and the HI column density.

© 2015 WILEY-VCH Verlag GmbH & Co. KGaA, Weinheim

1 Introduction

A connection between star formation and the spiral structure of disc galaxies is known since Morgan, Whitford & Code (1953) found concentrations of OB stars in the Sagittarius spiral arm of the Milky Way. This connection suggests that spiral arms trigger star formation. The development of the density-wave theory has shed new light on the connection between star formation and spiral arms. A density wave traveling through the disc of a galaxy produces a shock in the gas which should trigger formation of stars in spiral arms. Spiral arms are dense and promote more gravitational instabilities and cloud collisions than the interarm regions, triggering molecular cloud formation and conglomeration in the arms. This can easily explain the observed concentration of young stars in spiral arms.

Many studies of the spiral structure in galaxies compare various observational data in order to link star formation to spiral density waves in discs. These comparisons are mostly qualitative. There is a very illustrative diagram of Roberts, Roberts & Shu (1975) which relates the expected velocity of gas inflow into the spiral arm and the magnitude of the spiral arm shock with the morphological characteristics of the spiral structure and the van den Bergh luminosity classes. The earlier the luminosity class of the galaxy (i.e., the higher its luminosity), the brighter and more conspicuous are the spiral pattern it possesses. In this case, the galactic gas meets the spiral arm at a higher velocity. The higher this velocity,

the stronger the shock of gas and the higher the luminosity of the galaxy.

One can make a more detailed analysis by studying non-circular motions of gas clouds and stars caused by the spiral density wave in the disc of a galaxy. The perturbed velocities depend on the amplitude of the wave, the position of the corotation and the Lindblad resonances, and the mass distribution within the galaxy (the shape of rotation curve). The same parameters affect the radial behaviour of the velocity of gas inflow into the spiral arm, and thereby probably also the radial profile of SFR in the disc.

Previously, we compared a variation of the velocity of gas inflow, v_{\perp} , into the spirals and the surface density of star formation rate, Σ_{SFR} , in the disc with the galactocentric distance r in the spiral galaxy NGC 628 (Sakhibov & Smirnov 2004). We believe that the radial distribution of the SFR surface density, Σ_{SFR} , over the disc has a ring-like form with the maximum at the galactocentric distance $r \sim 3$ kpc, whereas the maximum of the velocity of gas inflow v_{\perp} is situated at $r \sim 5$ kpc. We derived the velocities of gas inflow v_{\perp} into the spirals at different galactocentric distances via a Fourier analysis of the azimuthal distribution of the observed radial velocities in annular (ring-like) zones of the disc of the NGC 628 and the radial profile of the surface density of SFR, using the empirical “SFR vs. linear size” relation for star formation complexes (Sakhibov & Smirnov 2004) and coordinates, H α fluxes, and the sizes of H II regions presented by Belley & Roy (1992).

The deviation between the maximum of the Σ_{SFR} in the disc at the $r \sim 3$ kpc and the maximum of the velocity of gas inflow v_{\perp} at $r \sim 5$ kpc shows that the total galactic star

* Corresponding author: gusev@sai.msu.ru

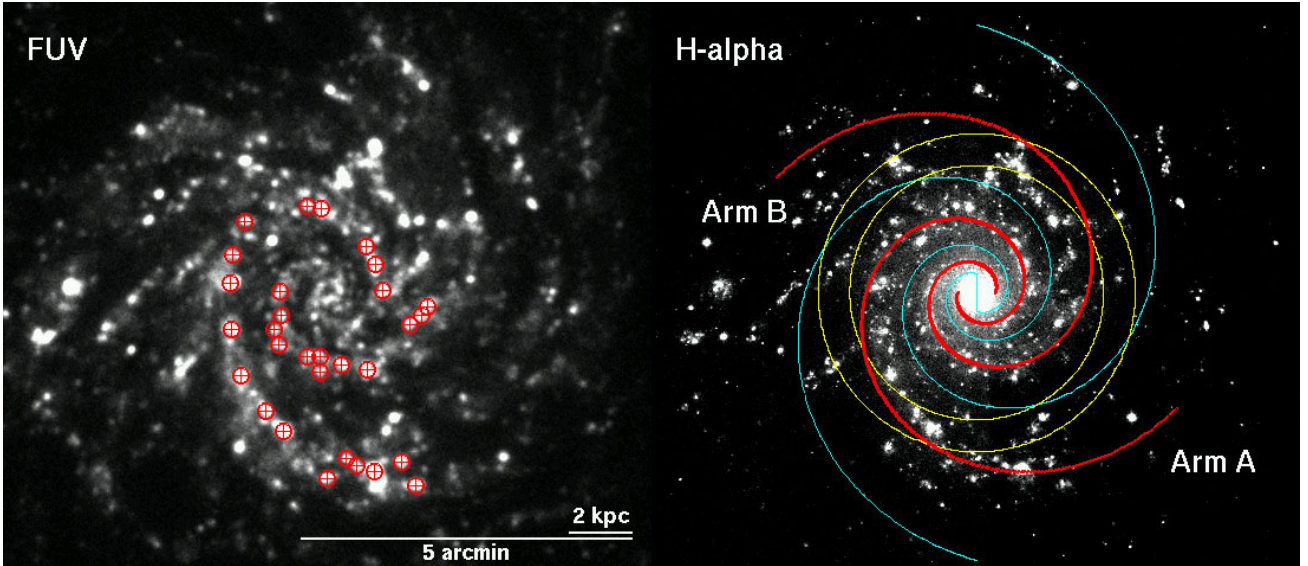


Fig. 1 Images of NGC 628 in the FUV (*left*) and H α line (*right*). The FUV image was taken from the GALEX archive, the H α image was obtained on the Maidanak Observatory with the 1.5 m telescope. Positions of star formation regions (red crosses in circles) from the list of Gusev et al. (2014) are indicated in the FUV image. Logarithmic spiral arms (thick red curves) and the boundary between two parts of the galaxy, around Arm A and Arm B (thin cyan curve) are shown in the H α line image. Yellow circles in the H α image have radii $r = 4$ and 5 kpc (see the text for details). North is upward and East is to the left.

Table 1 Basic parameters of NGC 628.

Parameter	Value
Type	SA(s)c
Total apparent B magnitude (B_t)	9.70 ± 0.26 mag
Absolute B magnitude (M_B) ^a	-20.72 mag
Inclination (i)	$7^\circ \pm 1^\circ$
Position angle (PA)	25°
Heliocentric radial velocity (v)	659 ± 1 km s ⁻¹
Apparent corrected radius (R_{25}) ^b	5.23 ± 0.24 arcmin
Apparent corrected radius (R_{25}) ^b	10.96 ± 0.51 kpc
Distance (d)	7.2 Mpc
Galactic absorption ($A(B)_{\text{Gal}}$)	0.254 mag
Distance modulus ($m - M$)	29.29 mag

^a Absolute magnitude of the galaxy corrected for Galactic extinction and inclination effect.

^b Isophotal radius (25 mag arcsec⁻² in the B -band) corrected for Galactic extinction and absorption due to the inclination of NGC 628.

formation rate in the main disc is not significantly enhanced by the presence of spiral arms (see Elmegreen 2010).

But the question remains open whether the peak of the velocity of gas inflow v_\perp into the spirals coincides with the peak of the radial distribution of the SFR within the spirals in the individual star formation regions.

Recently, Gusev & Efremov (2013) and Gusev, Egorov & Sakhibov (2014) investigated photometric properties of spiral arms in NGC 628, and the locations and parameters of star formation regions inside these arms. The thirty brightest star formation regions in the ultraviolet band, located in the spiral arms of NGC 628, were identified and stud-

ied (see Fig. 1). We found that the star formation regions in Arm A are systematically brighter and larger than the regions in Arm B (Gusev et al. 2014). We also measured the star formation rates (SFRs) and the surface densities (Σ_{SFR}) within these star formation regions using FUV magnitudes, H α luminosities, and sizes. Since the star formation rate per unit area is higher in the arms than in the main disc, we decide to study the relations between SFRs along the arms and the velocities of gas inflow into the spiral arms.

The main goal of this new research is to study relations between SFRs along the arms and the velocities of gas inflow into the spiral arms. This study is based on our own observations of the galaxy in the H α line, obtained at the Maidanak Observatory with the 1.5 m telescope, on Galaxy Evolution Explorer (GALEX) far-ultraviolet (FUV) data (Gusev & Efremov 2013; Gusev et al. 2014), as well as on a Fourier analysis of the spatial distribution of the radial velocities of the neutral gas in the disc (Sakhibov & Smirnov 2004).

Observations, data reduction, determination of parameters of spiral arms, selection criteria, and photometry of star formation regions have been described in detail in Gusev & Efremov (2013) and Gusev et al. (2014).

2 Previous studies of NGC 628

The spiral galaxy NGC 628 (M74) is one of the best studied nearby spiral galaxies viewed almost face-on (Fig. 1, Table 1). This prototypical grand-design galaxy hosts two principal arms. The first (south arm by Rosales-Ortega et al. 2011) is a long regular arm (Arm A in Fig. 1). In this arm, Elmegreen & Elmegreen (1983) found a regular string of

star complexes (H II regions). The shorter second arm (Arm B in Fig. 1) has a distorted outer part.

NGC 628 is an excellent example of a galaxy that has experienced recent star formation episodes. Hodge (1976) identified 730 H II regions in this galaxy. Ivanov et al. (1992) observed and compiled a catalogue of positions, angular sizes, integral magnitudes, and H II identification of 147 OB associations and aggregates in NGC 628. Numerous star formation regions have been studied earlier, based on photometric, spectroscopic, and spectrophotometric observations (McCall, Rybski & Shields 1985; Belley & Roy 1992; Ferguson, Gallagher & Wyse 1998; Bresolin, Kennicutt & Garnett 1999; Larsen 1999, 2004; Bruevich et al. 2007; Rosales-Ortega et al. 2011; Gusev et al. 2012; Berg et al. 2013).

The kinematics of the H I disc has been studied by Shostak & van der Kruit (1984) and Kamphuis & Briggs (1992). The neutral hydrogen distribution correlates with the optical structure within the optical disc. The H I velocity field beyond the optical edge can be ascribed to circular rotation in a plane (Shostak & van der Kruit 1984). Two giant high velocity gas complexes ($M(\text{H I}) \sim (0.5\text{--}1) \times 10^8 M_{\odot}$) are located at $\sim 10'$ to the east and to the west from the galactic centre (Kamphuis & Briggs 1992). The gas velocity dispersion as well as the stellar dispersion are typical for giant spiral galaxies, $\sigma(\text{H I}) = 8\text{--}10 \text{ km s}^{-1}$ at galactocentric distances, r , of $1.5'\text{--}3.5'$ (3.0–7.5 kpc for an adopted distance to NGC 628 of 7.2 Mpc; Shostak & van der Kruit 1984), $\sigma(\text{H II}) = 16\text{--}19 \text{ km s}^{-1}$ at r of $0.5'\text{--}2.7'$ (1.0–5.5 kpc) and $14 \pm 7 \text{ km s}^{-1}$ at r of $2.8'\text{--}4.0'$ (6.0–8.5 kpc; Fathi et al. 2007), and $\sigma(\text{stars}) = 50 \pm 20 \text{ km s}^{-1}$ at r of $0.3'\text{--}1.0'$ (0.7–2.0 kpc; MacArthur, González & Courteau 2009).

Although NGC 628 is a member of a small group of galaxies (Auld et al. 2006), it cannot have undergone any encounter with satellites or other galaxies in the past 1 Gyr (Wakker & van Woerden 1991; Kamphuis & Briggs 1992).

The rotation speed of the arms (pattern speed) is determined along with other parameters of the spiral-density wave (Sakhibov & Smirnov 2004) via a Fourier analysis of the azimuthal distribution of the observed radial velocities (Shostak & van der Kruit 1984) in annular zones of the disc of NGC 628. Comparison of the pattern speed with the pure circular motion of the gas provided the velocity of gas inflow into the spiral arm at different radial distances. The corresponding corotation radius is $R_{\text{cor}} \approx 7 \text{ kpc}$ (Sakhibov & Smirnov 2004).

The fundamental parameters of NGC 628 are presented in Table 1. We take the distance to NGC 628 as obtained in Sharina, Karachentsev & Tikhonov (1996) and van Dyk, Li & Filippenko (2006). We used the position angle and the inclination of the galactic disc as derived by Sakhibov & Smirnov (2004). The morphological type and the Galactic absorption, $A(B)_{\text{Gal}}$, are taken from the NED data base¹.

¹ <http://ned.ipac.caltech.edu/>

Other parameters are taken from the LEDA data base² (Paturel et al. 2003). We adopt the Hubble constant $H_0 = 75 \text{ km s}^{-1} \text{ Mpc}^{-1}$. With the assumed distance to NGC 628, we find a linear scale of $34.9 \text{ pc arcsec}^{-1}$.

3 Radial distributions of the star formation rates

We derived the radial distributions of SFRs in the galaxy using FUV and H α images of NGC 628. Previously, all data were corrected for Galactic absorption. Here we used the ratio of the extinction in the GALEX FUV band to the color excess $E(B - V)$: $A_{\text{FUV}}/E(B - V) = 8.24$ (Wyder et al. 2007) and the standard ratio $c(\text{H}\alpha) = 0.308A(V)$.

Azimuthally averaged photometric profiles of the galaxy in FUV and H α were obtained using round apertures in steps of $2''$. We do not transform images of NGC 628 to the face-on position, $i = 0^\circ$, because the position of any point in the galaxy is changed by a value much less than the characteristic width of the spiral arm if the adopted inclination $i = 7^\circ$ is considered. Differences between the uncorrected and corrected position is less than 0.5° for the inclination position angle and $\Delta r/r < 0.01$ for the galactocentric distance for any point in the galaxy.

For estimating SFR radial distribution peculiarities in the two opposite spiral arms of NGC 628, we divided the galactic image into two equal parts. The first part includes the area around Arm A, and the second part that around Arm B. We selected the boundary between the two parts using the parameters of symmetric logarithmic spirals obtained in Gusev & Efremov (2013). We determined the equation of the boundary at galactocentric distances $r \geq 21.95''$ as the equations of logarithmic spiral Arms A and B (see Gusev & Efremov 2013) that are rotated by 90° in the galactic plane. For the inner part of NGC 628, at $r < 21.95''$, the boundary lies on the north-south line (Fig. 1).

We adopt the conversion factor of the FUV luminosity to the star formation rate of Iglesias-Páramo et al. (2006):

$$\text{SFR}(M_{\odot} \text{ yr}^{-1}) = 8.13 \times 10^{-44} L_{\text{FUV}}(\text{erg s}^{-1}), \quad (1)$$

and the conversion factor of the H α luminosity to star formation rate of Kennicutt (1998):

$$\text{SFR}(M_{\odot} \text{ yr}^{-1}) = 7.9 \times 10^{-42} L_{\text{H}\alpha}(\text{erg s}^{-1}). \quad (2)$$

To estimate physical values of SFR along the spiral arms, we introduce the term ‘‘SFR per unit of length of a spiral arm’’, $\Delta\text{SFR}/\Delta l$. We adopt here that all the FUV and H α emission is concentrated in the thin spiral arms of the galaxy. For a logarithmic spiral with a pitch angle μ , the longitudinal displacement segment along the spiral, Δl , within a ring-like aperture with a width Δr is

$$\Delta l = \Delta r / \sin \mu, \quad (3)$$

² <http://leda.univ-lyon1.fr/>

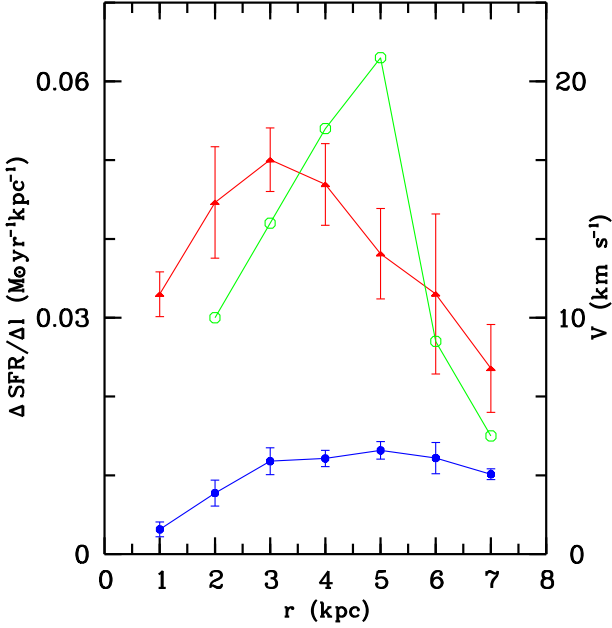


Fig. 3 Radial distributions of averaged values of $\Delta \text{SFR}/\Delta l$ for both arms, based on the luminosities in H α (red line and triangles) and FUV (blue line and circles). The $\Delta \text{SFR}/\Delta l$ averaged error bars are shown, too. The radial distributions of the velocities of gas inflow into the spiral arms (green line and open circles) after Sakhibov & Smirnov (2004) are also shown.

independently of the galactocentric radius. Gusev & Efremov (2013) obtained the pitch angle $\mu = 15.7^\circ$ for the arms. It is consistent with the estimations of Danver (1942) $\mu = 17^\circ \pm 2^\circ$ and close to the result of Kennicutt & Hodge (1976) who fitted each arm separately and obtained 13.8° for Arm A and 11.2° for Arm B. Thus, the values of $\Delta \text{SFR}/\Delta l$ were obtained using Eqs. (1), (2), and (3) with the constants $r = 2''$ (70 pc) and $\mu = 15.7^\circ$.

The radial distributions of $\Delta \text{SFR}/\Delta l$ are shown in Fig. 2 for Arms A and B separately. We also give the mean radial distributions for both arms in this figure. Additionally, we calculated the values of $\Delta \text{SFR}/\Delta l$, averaged over r in steps of 1 kpc. These data are also presented in Fig. 3.

The radial distributions show slightly higher SFRs in Arm A than in Arm B at galactocentric distances from 2 to 6 kpc. However, the distributions based on the FUV luminosities differ significantly from the ones based on H α emissions. The distribution of $\Delta \text{SFR}(\text{H}\alpha)/\Delta l$ has a clear maximum at $r \approx 3$ –4 kpc, the distribution of $\Delta \text{SFR}(\text{FUV})/\Delta l$ has a rather flat appearance between $r = 3$ –6 kpc (Fig. 3).

The values of $\Delta \text{SFR}(\text{H}\alpha)/\Delta l$ are 2–10 times larger than the values of $\Delta \text{SFR}(\text{FUV})/\Delta l$; their ratio decreases towards the outer part of NGC 628 (Fig. 3). These differences may be explained by the radial gradient of dust absorption in the disc of the galaxy. We roughly estimated parameters of the dust distribution based on the condition

$$\text{SFR}(\text{FUV})/\text{SFR}(\text{H}\alpha)(r) = 1.$$

The difference between the FUV and H α luminosity distributions shown in Fig. 3 can be explained by the gradient of dust absorption,

$$A(B) = 1.545 - 0.134r, \quad (4)$$

where r is the galactocentric distance in units of kpc. If the dust is uniformly mixed in the stellar and gaseous medium, the dust absorption $A(B)$ depends on the dust opacity, τ_B , as

$$A(B) = -2.5 \log[1 - \exp(-\tau_B)]/\tau_B \quad (5)$$

(Disney, Davies & Phillipps 1989).

Using Eqs. (4) and (5), we estimated the central opacity in the B band, $\tau_B \approx 3.9$, and the scale length of the dust disc, $h(B)_{\text{dust}} \approx 3.2$ kpc. The value of $h(B)_{\text{dust}}$ is close to the disc scale length in the B passband obtained by Möllenhoff (2004), who estimated $h(B) = 3.11$ kpc. The value of the central opacity in B is typical for dust opacities in central regions of local universe spiral galaxies according to Popescu et al. (2011) who found $\tau_B \sim 3.5$ –4. We also estimated the total dust mass using Eq. (44) from Popescu et al. (2011), $M_{\text{dust}} \approx 4 \times 10^7 M_\odot$. It is close to the last estimation of the dust mass in NGC 628. Aniano et al. (2012) found that $M_{\text{dust}} = (2.9 \pm 0.4) \times 10^7 M_\odot$ using data of *Spitzer* and *Herschel* (from $3.6 \mu\text{m}$ to $500 \mu\text{m}$).

Nevertheless, note that the radial distribution of the velocities of gas inflow into the spiral arms, v_\perp , poorly correlates with the distributions of SFRs based on both FUV and H α luminosities (Fig. 3).

4 Star formation rates within star formation regions and the radial distribution of the velocity of gas inflow into the spiral arms

To obtain the SFR, free from the dust influence, we used data of SFRs within star formation regions which were obtained for the 30 largest young stellar objects with known interstellar absorption in the regular parts of the spiral arms of NGC 628 in Gusev et al. (2014). These authors selected 30 star formation regions having a total magnitude, corrected for interstellar absorption, of $\text{FUV}_0 < 19.8$ mag. Among regions fainter than 19.8 mag in the FUV, we found a large number of diffuse objects without strong H α emission. Moreover, there are no measurements of interstellar absorption for such faint objects. We divided the star formation regions into several groups depending on their distances to the galactic centre with a step of 1 kpc. For every group, the average SFR, $\langle \text{SFR} \rangle$, was calculated as

$$\langle \text{SFR} \rangle = \frac{1}{n} \sum_n \text{SFR}_n, \quad (6)$$

where n is a number of objects in the group and SFR_n is the SFR within the n -th object. These mean SFRs were obtained separately for Arm A and Arm B, based on both FUV and H α data (Fig. 4). We also calculated the mean SFRs for both FUV and H α luminosities, $(\langle \text{SFR}(\text{FUV}) \rangle + \langle \text{SFR}(\text{H}\alpha) \rangle)/2$.

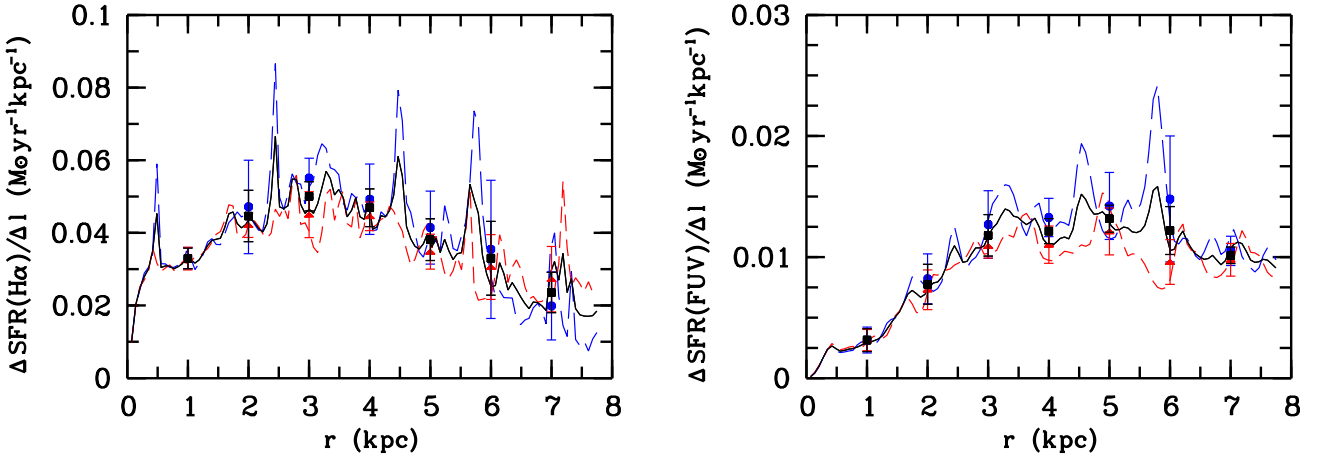


Fig. 2 Radial distributions of SFRs per unit of length of the spiral arm, $\Delta\text{SFR}/\Delta l$, based on the luminosities in $\text{H}\alpha$ (*left panel*) and FUV (*right panel*), and their averaged values for Arm A (blue long-dashed curves and circles), Arm B (red short-dashed curves and triangles), and the mean for both arms (black solid curves and squares). The $\Delta\text{SFR}/\Delta l$ averaged error bars are shown.

Note that the total SFR of the studied 30 regions, $\approx 0.25 \text{ M}_{\odot} \text{ yr}^{-1}$, is a significant part (one third) of the total SFR in NGC 628, $0.7 \pm 0.2 \text{ M}_{\odot} \text{ yr}^{-1}$ (Calzetti et al. 2010).

Similarly, we calculated the mean values of the SFR surface density within the star formation regions, $\langle \Sigma_{\text{SFR}} \rangle$, given by

$$\langle \Sigma_{\text{SFR}} \rangle = \frac{4}{\pi} \left\langle \frac{\text{SFR}}{d^2} \right\rangle, \quad (7)$$

where the diameters of star formation regions, d , were obtained in Gusev et al. (2014).

Arm B is distorted for galactocentric distances $r > 3.2$ kpc (Fig. 1). We did not measure the luminosities of star formation regions in the distorted part of Arm B. As a result, the radial distributions of $\langle \text{SFR} \rangle$ and $\langle \Sigma_{\text{SFR}} \rangle$ within the star formation regions in Arm B were constructed up to $r \approx 3$ kpc only.

As seen from Fig. 4, the values and the distributions of $\langle \text{SFR} \rangle$ and $\langle \Sigma_{\text{SFR}} \rangle$ obtained from FUV and $\text{H}\alpha$ data are close to each other. The mean SFR in the star formation regions of Arm A is comparable within the errors with the mean SFR in the star formation regions of Arm B.

The distribution of the mean SFR within star formation regions in Arm A correlates with the distribution of the velocities of gas inflow into the spiral arm very well. Both distributions have a clear maximum at $r = 5$ kpc. The mean surface density of SFRs within star formation regions does not correlate with v_{\perp} , and is approximately constant for $r = 3-6$ kpc, $\langle \Sigma_{\text{SFR}} \rangle = 0.06-0.09 \text{ M}_{\odot} \text{ yr}^{-1} \text{ kpc}^{-2}$, and decreases towards the corotation region of NGC 628 (Fig. 4).

The difference between the radial distributions of $\langle \text{SFR} \rangle$ and $\langle \Sigma_{\text{SFR}} \rangle$ is due to the fact that the star formation regions in Arm A at the galactocentric distances $4 \text{ kpc} < r < 6 \text{ kpc}$ are larger and brighter than those in the inner and outer parts of the arm.

A small number of objects in our sample which contains only bright star formation regions makes it impossible to determine the maximum in the radial distribution of the SFR

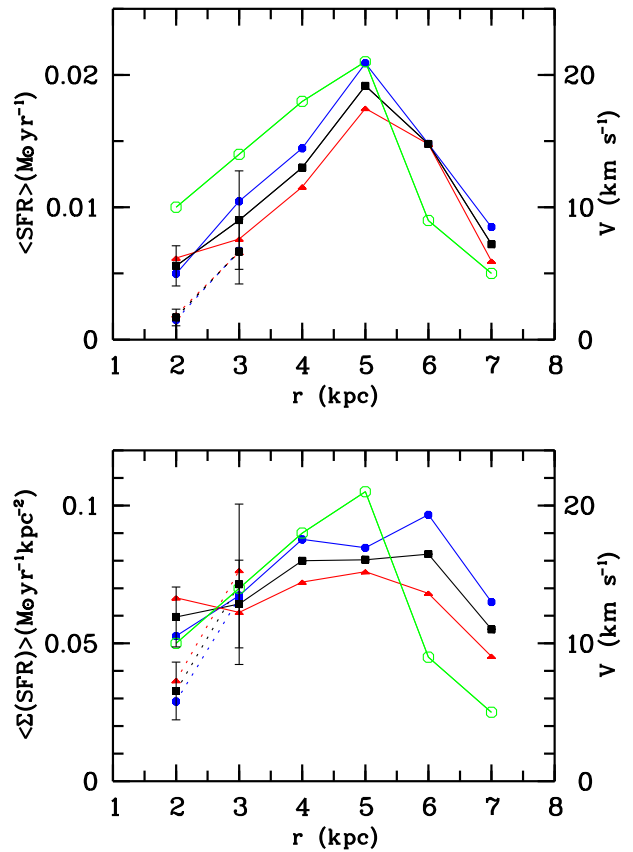


Fig. 4 Radial distributions of the mean SFR (*top*) and the mean surface density of SFRs (*bottom*) within star formation regions based on their luminosities in FUV (blue lines and circles), $\text{H}\alpha$ (red lines and triangles), and the mean for both luminosities (black lines and squares) in Arm A (solid lines) and Arm B (dotted lines). Radial distributions of the velocities of gas inflow into the spiral arms (green solid curves and open circles) are also shown. The $\langle \text{SFR} \rangle$ and $\langle \Sigma_{\text{SFR}} \rangle$ error bars are shown for Arm A and Arm B.

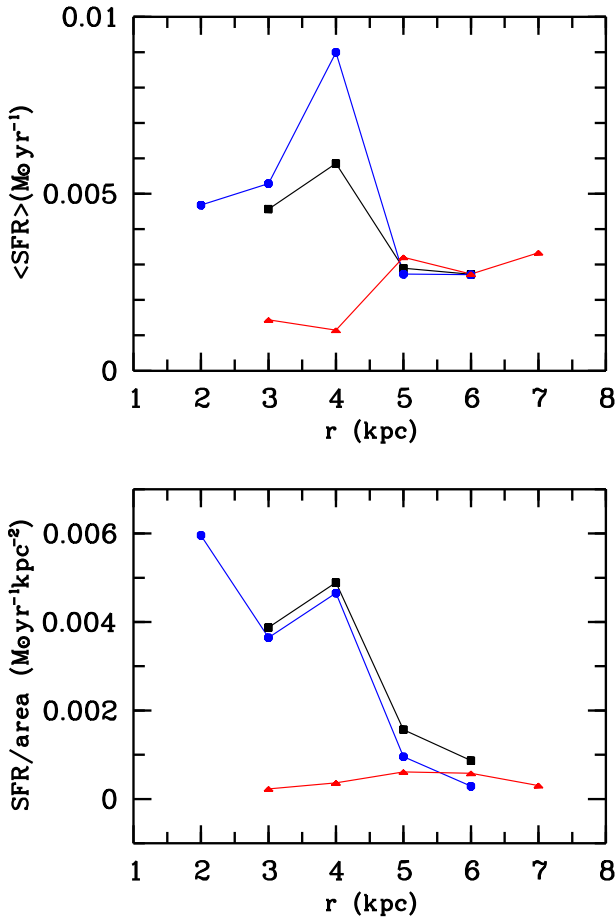


Fig. 5 Radial distributions of the mean SFR (*top*) and the total SFR per square kpc (*bottom*) within star formation regions based on their luminosities in H α according to Rosales-Ortega et al. (2011). Distributions of SFRs within star formation regions in spiral arms (blue lines and circles), within star formation regions outside spiral arms in the main disc (red lines and triangles), and within all star formation regions (black lines and squares) are shown.

with an accuracy less than ± 1 kpc. Therefore, we additionally examined a sample of H II regions from Rosales-Ortega et al. (2011) containing 96 objects inside and outside the spiral arms of the galaxy. The results of the analysis of this sample are presented in Fig. 5. Here, we calculated the average SFR using Eq. (6). In contrast to the bottom panel of Fig. 4 where we plotted the profile of the mean SFR within star formation regions per area occupied by a star formation region and calculated by Eq. (7), we present in the bottom panel of Fig. 5 the profile of the total SFR within star formation regions per galaxy area, averaged over r ,

$$\text{SFR}/\text{area} = \sum_n \text{SFR}_n / \pi [(r + 0.5)^2 - (r - 0.5)^2],$$

where r is a galactocentric distance in units of kpc. Only two objects in the spiral arms have $r = 7 \pm 0.5$ kpc, and two star formation regions outside the spiral arms are located at distances $r = 2 \pm 0.5$ kpc. We do not show data for them in Fig. 5.

As seen from Figs. 4 and 5, the maximum of the distribution of the mean SFR within star formation regions in spiral arms by Rosales-Ortega et al. (2011) is shifted relative to the maximum of the distribution of the mean SFR within star formation regions in Arm A by our data (4 kpc versus 5 kpc). The basic reason of this shift is the presence of several bright H II complexes which are located in Arm B in the northern-western part of NGC 628; these complexes are located at $r \approx 4\text{--}4.5$ kpc (Fig. 1). The largest and brightest H α complex, No. 40, of Rosales-Ortega et al. (2011) is also located here. Moreover, a significant contribution to the increase in $\langle \text{SFR} \rangle$ is made by one of the brightest star formation regions, No. A12 (Gusev et al. 2014) or 84 (Rosales-Ortega et al. 2011), which is located at $r \approx 4.5$ kpc. The estimated galactocentric distance to his centre is 4.60 kpc, but Rosales-Ortega et al. (2011), however, gave a distance of $r = 4.43$ kpc.

The shift of the absolute values of the mean SFR between the distributions based on our data and the data of Rosales-Ortega et al. (2011) is due to the fact that the sample of Rosales-Ortega et al. (2011) contains more H II regions than ours and includes fainter regions not included in our sample.

Note that the maximum velocity of gas inflow into the spiral arms is apparently achieved at distances $r \sim 4.5\text{--}5.0$ kpc, as can be seen from the velocity graph in Fig. 4.

The total SFR within star formation regions in spiral arms per galaxy area decreases considerably with increasing distance from the centre of the galaxy (bottom panel of Fig. 5). Nevertheless, the increase in star formation rate at $r = 4$ kpc is seen clearly in the figure.

Radial distributions of the mean and total SFRs within star formation regions inside and outside the spiral arms are significantly different from each other (Fig. 5). Both $\langle \text{SFR} \rangle$ and total SFR per galaxy area within star formation regions in spiral arms have obvious maxima at $r \approx 4$ kpc, and they decrease towards $r \sim 6$ kpc. $\langle \text{SFR} \rangle$ and the total SFR within star formation regions outside the spiral arms grow from 4 to 6 kpc (Fig. 5). Both $\langle \text{SFR} \rangle$ and total SFR per galaxy area within star formation regions become equal to each other for objects inside and outside the spiral arms at $r \approx 6$ kpc.

Obviously, star formation parameters depend on the properties of the interstellar medium. The key ingredient of star formation is molecular hydrogen. However, molecular hydrogen is concentrated in the central part of galaxies. In contrast to H₂, the density of neutral hydrogen decreases towards the centre (a deficiency of H I is typically observed at the distance of a few kpc from the centre). We examined the radial distribution of the H I column density in NGC 628 based on the 21 cm line image obtained in Walter et al. (2008). The image³ was downloaded from the NED data base (Fig. 6). Heiner et al. (2013) estimated the atomic hydrogen column densities in H I patches in the spiral arms associated with photodissociation regions in NGC 628. The

³ Original image: NGC_628_RO_MOM0:1:HI:wbb2008.fits

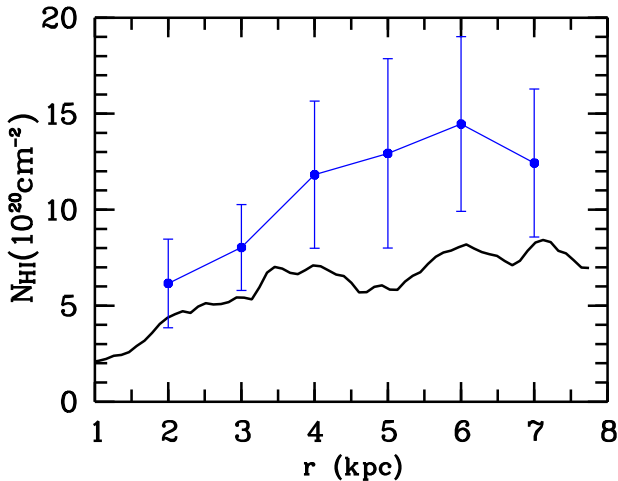


Fig. 6 Radial distributions of H I column density (thick black curve) and the mean H I column density in H I patches in spiral arms associated with photodissociation regions (blue lines and circles). The N_{HI} averaged error bars are shown.

radial distribution of the mean H I column density in these H I patches, averaged over r , is also presented in Fig. 6.

As seen from Fig. 6, typical N_{HI} values in H I patches are 1.5–2 times larger than the values averaged azimuthally. However, their profiles are similar to each other; the H I column densities increase up to galactocentric distances of 3–4 kpc and have plateau-like profiles at $r = 4$ –7 kpc. These profiles do not coincide with the profiles of the radial distribution of $\langle \text{SFR} \rangle$ and total SFR per galaxy area within star formation regions in spiral arms of the galaxy (Figs. 5 and 6).

5 Discussion

We would like to underline the important result derived in this paper: The peak of the orthogonal component of the velocity of gas inflow into the spiral arms, v_{\perp} , coincides with the peak of the radial distribution of the mean SFR within the individual star formation regions. Both peaks are placed within the regular spiral arms at the galactocentric distance $r \approx 4.5$ –5.0 kpc, where the component of the difference between the spiral pattern and gas velocities, that is orthogonal to the arm, is maximal.

This result confirms the prediction of the density wave theory illustrated in Roberts et al. (1975). Sakhibov & Smirnov (2004) showed similar radial distributions of the velocity of gas inflow and the surface density of the SFR in another nearby spiral galaxy, NGC 6946. The maximum of the velocity of gas inflow and the peak of the SFR are at the same radial distance $r \approx 4$ kpc from the centre of the galaxy, between the inner Lindblad resonance (~ 2.5 kpc) and the corotation radius (~ 9 kpc) (Sakhibov 2004).

A similar situation was noted in the SW arm of M31, where a stellar age gradient across this arm segment is clearly observed, being evident due to the unusually large

pitch angle of this arm segment (Efremov 2010), whereas the pitch angle is close to zero for almost all other arms of M31. According to the classical theory (Roberts et al. 1975), the degree of gas compression by a spiral shock wave is determined by the component v_{\perp} of the difference between the velocities of solid-body rotation of the density wave (Vdw) and differential rotation of the galaxy's gas, V , around the centre. The component v_{\perp} is perpendicular to the wave front, i.e. to the inner boundary of the arm: $v_{\perp} = (V - Vdw) \sin \mu$ (see Efremov 2010).

It implies that at the same distance from the co-rotation (where $V = Vdw$), the shock wave should be stronger in the arm segment with the larger pitch angle. The shock wave compresses gas clouds; the higher the density of the initial gas cloud, the higher the effectiveness of star formation. The large pitch angle of the arm segment in question leads to a high value of v_{\perp} (see Fig. 1).

Peaks in the radial distribution of the gas inflow velocity into the spiral arms, as well as in the mean SFR within star formation regions in spiral arms do not coincide with the peak of the radial distribution of the H α luminosity in the galaxy at $r \approx 3$ kpc. Apparently, this difference may be explained by the radial gradient of dust absorption in the disc of NGC 628 as well as by diffuse radiation of H α in the central part of the galaxy.

On the other hand, the radial distributions of the mean and total SFRs in the individual star formation regions inside and outside the spiral arms significantly differ from each other (Fig. 5). This result confirms the conclusion made previously by Elmegreen (2011) that the total galactic star formation rate in the main disc is not significantly enhanced by the presence of spiral arms.

The mean surface density of SFR within star formation regions is approximately constant at distances from 3 to 6 kpc from the centre of NGC 628 (Fig. 4). Obviously, the mean surface density of the SFR within star formation regions, Σ_{SFR} , depends basically on the general properties of the interstellar medium such as gas density and pressure.

Both the mean and the total SFRs within star formation regions become equal to each other for the objects inside and outside the spiral arms in the outer part of NGC 628 at $r > 5$ kpc (Fig. 5). These regions are situated in the vicinity of the corotation radius, $R_{\text{cor}} \approx 7$ kpc, where the velocity of the spiral pattern coincides with the rotation velocity of the galaxy. Dynamic properties of interstellar matter inside and outside the spiral arms must be close to each other in this region.

We note in conclusion, that, as Martínez-García & Puerari (2014) have noted, most of a dozen galaxies without signatures of density-formed spiral pattern (Foyle et al. 2011) have spiral arms of the flocculent and multi-arm type (apart from NGC 628 and NGC 5194). These galaxies are not described by the density wave theory.

6 Conclusions

We found a correlation between the mean SFR within individual star formation regions in the regular parts of spiral arms and the velocity of gas inflow into the spiral arms in the grand-design galaxy NGC 628. Both quantities reach a maximum at a distance of 4.5–5 kpc from the centre of the galaxy.

Radial distributions of SFRs within star formation regions inside and outside the spiral arms are not correlated with each other. However, both the mean and the total SFRs within star formation regions become approximately equal to each other for the objects inside and outside the spiral arms in the outer part of NGC 628 at a distance of $r \sim 6$ kpc, near the corotation radius.

The mean surface density of the SFR within star formation regions is approximately constant at distances from 3 to 6 kpc from the centre of NGC 628.

Acknowledgements. We are grateful to the referee for his/her constructive comments. The authors thank A.V. Zasov (SAI MSU) for helpful discussions and E.V. Shimanovskaya (SAI MSU) for help with the editing of this paper. The authors acknowledge the usage of the HyperLeda data base (<http://leda.univ-lyon1.fr>), the NASA/IPAC Extragalactic Database (<http://ned.ipac.caltech.edu>), B.A. Miculski archive for space telescopes (<http://galex.stsci.edu>), and the Padova group online server CMD (<http://stev.oap.inaf.it>). This study was supported by the Russian Science Foundation (project no. 14–22–00041).

References

- Aniano, G., Draine, B.T., Calzetti, D., et al. 2012, *ApJ*, 756, 138
- Auld, R., Minchin, R.F., Davies, J.I., et al. 2006, *MNRAS*, 371, 1617
- Belley, J., & Roy, J.-R. 1992, *ApJS*, 78, 61
- Berg, D.A., Skillman, E.D., Garnett, D.R., et al. 2013, *ApJ*, 775, 128
- Bresolin, F., Kennicutt, R.C., & Garnett, D.R. 1999, *ApJ*, 510, 104
- Bruevich, V.V., Gusev, A.S., Ezhkova, O.V., Sakhibov, F.Kh., & Smirnov, M.A. 2007, *Astron. Rep.*, 51, 222
- Calzetti, D., Wu, S.-Y., Hong, S., et al. 2010, *ApJ*, 714, 1256
- Danver, C-G. 1942, *Ann. of the Observatory of Lund*, 10, 3
- Disney, M., Davies, J., & Phillipps S. 1989, *MNRAS*, 239, 939
- Efremov, Yu.N. 2010, *MNRAS*, 405, 1531
- Elmegreen, B.G. 2011, in *Ecole Evry Schatzman 2010: Star Formation in the Local Universe*, eds. C. Charbonnel & T. Montmerle, EAS Publications Series, 51, 19
- Elmegreen, B.G., & Elmegreen, D.M. 1983, *MNRAS*, 203, 31
- Fathi, K., Beckman, J.E., Zurita, A., et al. 2007, *A&A*, 466, 905
- Ferguson, A.M.N., Gallagher, J.S., & Wyse, R.F.G. 1998, *AJ*, 116, 673
- Foyle, K., Rix, H.-W., Dobbs, C.L., Leroy, A.K., & Walter, F. 2011, *ApJ*, 735, 101
- Gusev, A.S., & Efremov, Yu.N. 2013, *MNRAS*, 434, 313
- Gusev, A.S., Egorov, O.V., & Sakhibov, F. 2014, *MNRAS*, 437, 1337
- Gusev, A.S., Pilyugin, L.S., Sakhibov, F., et al. 2012, *MNRAS*, 424, 1930
- Heiner, J.S., Sánchez-Gallego, J.R., Rousseau-Nepton, L., & Knapen, J.H. 2013, *MNRAS*, 428, 3355
- Hodge, P.W. 1976, *ApJ*, 205, 728
- Iglesias-Páramo, J., Buat, V., Takeuchi, T.T., et al. 2006, *ApJS*, 164, 38
- Ivanov, G.R., Popravko, G., Efremov, Yu.N., Tichinov, N.A., & Karachentsev, I.D. 1992, *A&AS*, 96, 645
- Kamphuis, J., & Briggs, F. 1992, *A&A*, 253, 335
- Kennicutt, R.C. 1998, *ARA&A*, 36, 189
- Kennicutt, R.C., & Hodge, P.W. 1976, *ApJ*, 207, 36
- Larsen, S.S. 1999, *A&AS*, 139, 393
- Larsen, S.S. 2004, *A&A*, 416, 537
- MacArthur, L.A., González, J.J., & Courteau, S. 2009, *MNRAS*, 395, 28
- Martínez-García, E.E., & Puerari, I. 2014, *ASPC*, 480, 137
- McCall, M.L., Rybski, P.M., & Shields, G.A. 1985, *ApJS*, 57, 1
- Möllenhoff, C. 2004, *A&A*, 415, 63
- Morgan, W.W., Whitford, A.E., & Code, A.D. 1953, *ApJ*, 118, 318
- Paturel, G., Petit, C., Prugniel, Ph., et al. 2003, *A&A*, 412, 45
- Popescu, C.C., Tuffs, R.J., Dopita, M.A., et al. 2011, *A&A*, 527, A109
- Roberts, W.W., Roberts, M.S., & Shu, F.H. 1975, *ApJ*, 196, 381
- Rosales-Ortega, F.F., Diaz, A.I., Kennicutt, R.C., & Sanchez, S.F. 2011, *MNRAS*, 415, 2439
- Sakhibov F. 2004, D. Sc. Thesis, Lomonosov Moscow State University
- Sakhibov, F.Kh., & Smirnov, M.A. 2004, *Astron. Rep.*, 48, 995
- Sharina, M.E., Karachentsev, I.D., & Tikhonov, N.A. 1996, *A&AS*, 119, 499
- Shostak, G.S., & van der Kruit, P.C. 1984, *A&A*, 132, 20
- van Dyk, S.D., Li, W., & Filippenko, A.V. 2006, *PASP*, 118, 351
- Wyder, T.K., Martin, D.C., Schiminovich, D., et al. 2007, *ApJS*, 173, 293
- Wakker, B.P., & van Woerden, H. 1991, *A&A*, 250, 509
- Walter, F., Brinks, E., de Blok, W.J.G., et al. 2008, *AJ*, 136, 2563